



Using *in operando* diffraction to relate lattice strain with degradation mechanism in a NMC battery

Shikhar Krishn Jha^{1,*} , Harry Charalambous¹ , John S. Okasinski² , and Thomas Tsakalakos¹ 

¹Department of Materials Science and Engineering, Rutgers University, Piscataway, NJ 08854, USA

²Argonne National Laboratory, Advanced Photon Source, Lemont, IL 60439, USA

Received: 25 July 2018

Accepted: 8 October 2018

Published online:

12 October 2018

© Springer Science+Business Media, LLC, part of Springer Nature 2018

ABSTRACT

Crystallographic structural changes in a commercial 5 Ah prismatic graphite–NMC battery were investigated during its operation using energy-dispersive X-ray diffraction. The characteristic diffraction peaks for the anode and cathode were identified, and their peak positions were linked to the charge–discharge cycle of the battery. The edge of the negative terminal of battery was shown to undergo irregular cycling behavior. Stresses developed at the battery layer interfaces were proposed to be the source for this deterioration, which limits the lifetime of the battery. The effect of pulse discharge on strain in cathode has also been studied.

Introduction

Development of hybrid and fully electric vehicles reduces the consumption of non-renewable energy sources, but requires the development of high-capacity, lightweight batteries with high reliability and long lifetimes. The materials used for these batteries have evolved over time from lead acid (General Motors EV1, 1996–1999) to Nickel–Cadmium to Nickel metal hydride and currently to Li-ion batteries (Tesla Model S and Nissan Leaf) [1]. Li-ion batteries have a number of advantages over the aforementioned types: highest energy density (100–265 Wh/kg), higher voltage to deliver the current needed for high-power applications, low current leakage rates

and the absence of the ‘memory effect’ as found in Nickel–Cadmium batteries, wherein repeated partial charge–discharge cycles result in lower battery capacity. The absence of ‘memory effects’ provides flexibility in operation by allowing partial charge–discharge of the battery rather than requiring a full discharge before recharging. All of these factors make Li-ion batteries a desirable choice for electric vehicles.

While Li-ion batteries are used ubiquitously in consumer applications, such as laptops and mobile phones, their successful adoption by the automotive industry has been difficult due to expectations of 2000 cycles over 5 years of operation [2] in order to be economically viable at the current cost of battery manufacturing. There exists a gap between the expectations of battery performance and the reality,

Shikhar Krishn Jha and Harry Charalambous have contributed equally to this paper.

Address correspondence to E-mail: jhashikhar@gmail.com

as batteries tend to fail prematurely due to the complexity of the design required for scaling up energy storage capacity [3–7]. Current Li-ion batteries are intricately designed, multilayered, multimaterial devices that rely on concurrent electronic and mass transfer during operating cycles. High-capacity and energy-density requirements make assembly of the battery complicated. Many factors have been identified for the early end-of-life of a Li-ion battery, such as dendritic growth of lithium, oxidation of the electrolyte at the cathode leading to capacity loss, aging mechanisms [4, 8, 9], growth of solid electrolyte interphase (SEI) [8], which block the graphitic anode, formation of dead zones in the battery, porosity and thickness of the electrodes, mechanical design parameters, delamination of layers, permanent deformation, thermal exposure [10, 11] and other unknown mechanisms active during the operation of the battery. Considering all these factors, batteries are often built to overcapacity to meet minimum expectations of performance over extended periods of time. Reducing these performance losses offers an opportunity to reduce the overcapacity requirements, so it becomes crucial to identify the mechanism(s) responsible for early degradation.

One challenge to improving battery efficiency is that the electrode materials are inaccessible once they are packaged, thus limiting the ability to determine battery failure mechanisms. Impedance spectroscopy or voltage–current cycle data can be obtained [11], but they do not reveal the effect of localized structural changes during the cycle. Another option is the use of destructive testing, but it is not always suitable since the same battery cannot be used for further testing and ex situ measurements of the electrodes do not capture the actual electrochemical dynamics present during its operation. Once the battery is brought to its rest state, the microstructure relaxes due to the fast diffusion kinetics of lithium. Additionally, removing the components from the device itself may alter the material state that is provided by the casing.

X-ray diffraction is commonly used to identify and quantify crystalline materials. Mechanical and electrochemical strain in materials can be determined by comparing the measured lattice parameters against a reference state. Recently, in situ X-ray and neutron diffraction has been successfully used to study the structural changes in electrodes during battery operation [2, 12–18]. Energy-dispersive X-ray

diffraction (EDXRD) is among these in situ methods, previously used as a nondestructive method to understand the state of stress and strain of engineered components [19–22]. The EDXRD measurements are taken using a transmission geometry and provide spatial and temporal mapping capabilities. High-energy X-rays can penetrate through tens of centimeters of material and isolate a discrete volume within the battery to quantify the local strain. A collimated X-ray beam with a broad spectrum of wavelengths impinges on the sample and scatters into a solid-state detector [23]. The detector simultaneously collects the intensity of different wavelengths to capture a range of diffraction peaks corresponding to different energies. Upon rearranging Bragg's Law and substituting wavelength λ with energy, E , Eq. 1 is obtained, which converts energy of radiation with constructive diffraction peak into the corresponding interplanar spacing.

$$E = \frac{hc}{2\text{Sin}\theta} \left(\frac{1}{d_{hkl}} \right) \quad (1)$$

Paxton et al. [23, 24] demonstrated the use of this method for the spatial distribution of electrochemical materials in the battery. However, it is worth noting that while EDXRD provides advantages over monochromatic diffraction in terms of isolating the measured data to a small gauge volume, it also has shortcomings, such as non-uniform absorption for different wavelengths which makes this method unsuitable for Rietveld analysis [25]. Rietveld refinement uses the least-squares fitting method and refines the theoretical line profile to match with the experimentally obtained pattern. This analysis helps to determine the peak broadening because of strain in the lattice and changes in grain-size as well as possible texture in the material. In the case of EDXRD, unlike monochromatic radiation, a spectrum of white-light X-ray radiation is used and the intensity of certain wavelengths matches the diffraction condition. However, there are two problems with this configuration: (a) The intensity of incident X-rays are not the same for all wavelengths and (b) the absorption of X-rays by the material is wavelength dependent. It is important to note that for a small energy range, such as for a single diffraction peak, these factors have minimal effect on the individual peak's shape, allowing accurate estimation of the interplanar spacing.

In the current study, the EDXRD technique is used to understand the deterioration mechanisms operating in different parts of a graphite–NMC ($\text{Li}_x\text{Ni}_{1/3}\text{Mn}_{1/3}\text{Co}_{1/3}\text{O}_2$) battery by following the structural change in the lattice parameters of the electrodes and current collectors during operation. The mapping of spatial inhomogeneity of component material strains is used to identify the role of internal strain in the early demise of certain sections of the battery assembly during current cycling.

Experimental details

Battery design

Among the commercially available batteries for automotive electric vehicles, a 5 Ah graphite–Li–NMC ($\text{Li}_x\text{Ni}_{1/3}\text{Mn}_{1/3}\text{Co}_{1/3}\text{O}_2$) prismatic cell was chosen for this study. The schematic of the battery assembly has been shown in Fig. 1a, c. Layers of anode, cathode, separator and current collectors were flattened by a mechanical press and submerged in a bath of liquid electrolyte. The electrode layers were comprised of aluminum and copper foils coated on both sides by cathode and anode, respectively. The metallic current collectors, copper and aluminum, extend out and were crimped and connected to the battery terminals. The assembly was sealed in a steel case.

Energy-dispersive X-ray diffraction (EDXRD)

The 2θ angle was chosen to be 3° in order to allow for the X-ray spectrum to match with the d -spacings of the diffraction peaks of interest. The experiments were carried out at the 6-BM-A beamline of the Advanced Photon Source at Argonne National Laboratory. This beamline is designed for phase transformation and mapping as well as strain mapping analysis in engineering components [26]. A bending magnet source generates a broad spectrum of incident beam X-rays with a useable spectral flux of up to 250 keV. The height and width of the incident X-ray beam was kept constant ($0.2 \text{ mm} \times 1.0 \text{ mm}$) for *in-plane* and *out-of-plane* measurements. As a battery has a lamellar structure, the strain developed in the perpendicular direction would differ from strain in the plane of layered sheets. The diffraction vector limits

the diffraction only from the grains with a particular orientation. This comparison of *in-plane* and *out-of-plane* measurements enables differentiation of the strain developed in two directions. A micro-positioning X–Y–Z stage translated the battery cell so that the diffraction gauge volume probed different locations of the battery. A Canberra germanium solid-state detector collected the diffracted spectra from the sample using a transmission geometry with an acquisition time of 60 s per scan. This rate of acquisition was required to obtain sufficient counts from relatively faint peaks, since the X-rays are highly attenuated due to the 120 mm length of steel casing and battery materials. The detector output spectra were converted into energy and d -spacing of different materials using reference diffraction spectra standards. A program was developed in MATLAB® to automate the data processing and peak fitting. The error is calculated for the peak fitting with 95% confidence interval. The height of the error for strain in NMC (101) is too small ($\sim 0.005\%$) to be visible in the plot. Of course, the error in fitting depends on the peak counts, so the stronger the peak the smaller the error. Thus, the NMC (101) peaks, which have highest intensity, are compared to understand the change in lattice parameters during the battery's operation.

Battery data acquisition

During the measurements, the battery was cycled through the charge–discharge routine at two rates, 1 C at 5 A for 1 h and a fast discharge of 4 C at 20 A for 5 min, using an Arbin battery cyler. The electrical parameters, voltage and current, during a charge–discharge cycle are shown in Fig. 2a. A complete XRD plot for an entire cycle is shown in a contour plot in Fig. 2b, where the y -axis corresponds to energy, the x -axis to time, and the color to intensity. A slice of this plot gives an XRD pattern at a particular time which can be converted into interplanar spacing as shown in Fig. 2c. The peaks have been identified using powder diffraction pattern (PDF) cards corresponding to Li–NMC (No. 00-062-0431), delithiated Li–NMC ($\text{Li}_{0.63}$ (No. 01-075-3918), $\text{Li}_{0.58}$ (No. 01-075-3919) and $\text{Li}_{0.48}$ (No. 01-075-3920)), aluminum (No. 04-012-7848), copper (No. 04-009-2090), graphite (No. 00-056-0159) and lithiated graphite (LiC_6 (No. 01-083-4148), LiC_{12} (No. 01-083-4147) and LiC_{24} [2]. Table 1 shows the Miller indices and interplanar spacing of different materials.

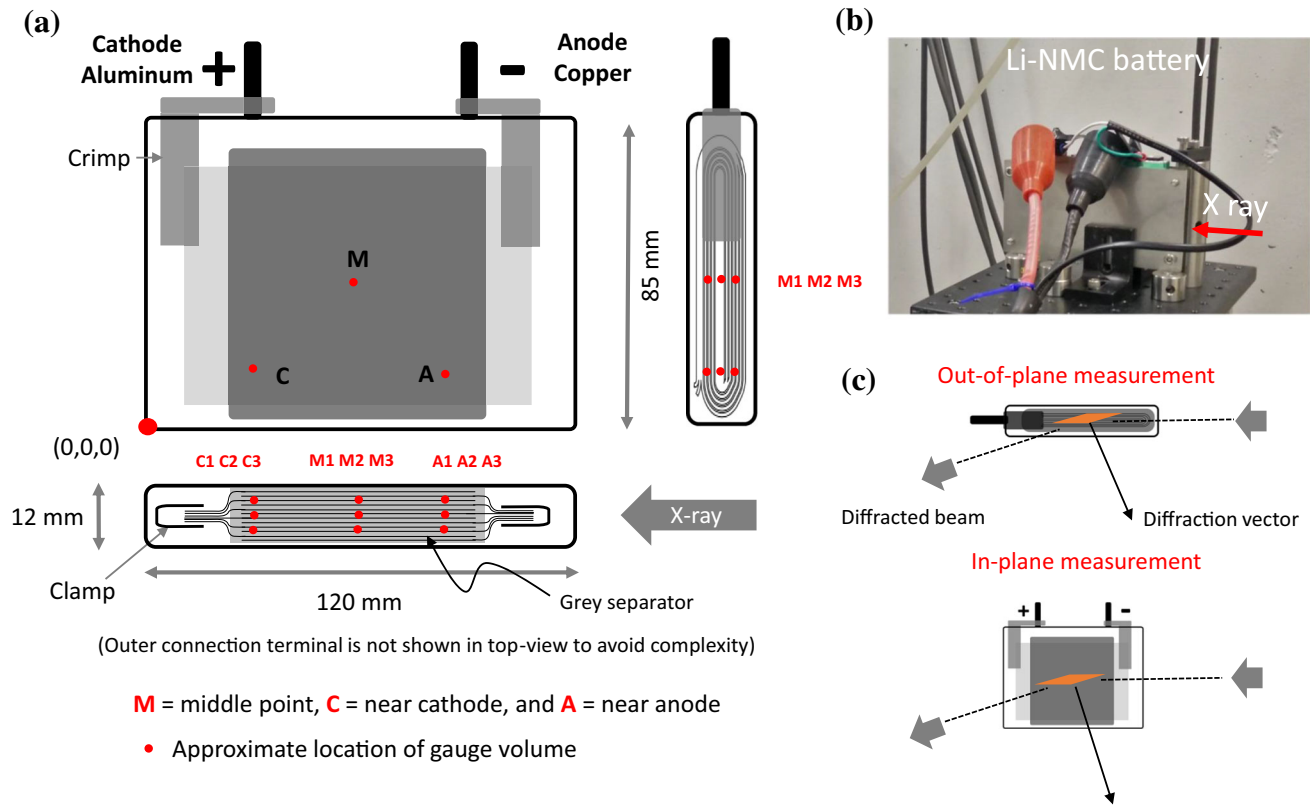


Figure 1 a Schematic design of Li-NMC battery and b the experimental setup at the synchrotron. Three points have been taken for analysis at the middle (M), cathode (C) and anode ends

Unfortunately, the two measured peaks for aluminum overlap with two of the peaks for NMC and could not be resolved.

Since the beam time at the synchrotron source is limited, the complete set of experiments was performed over three visits, each separated by 4 months. In the first visit, out-of-plane XRD measurements were taken at point M2 (refer to Fig. 1a). In the second run, three points (gauge volumes) were selected across the thickness at three different locations (middle, anode and cathode). A total of nine scans of the battery were collected for the *in-plane* configuration. In the third visit, a macro was written to scan the thickness profile of the battery *in-plane* with each point separated by 2 mm. Once the thickness profile was completed, the stage moved back to its initial position and the next profile was initiated. This procedure continued until a total of 23 scans were taken for each of the six positions across the thickness of the battery during a complete charge-rest-discharge cycle of 130 min. This schedule was followed for the three

(A) of the battery. c Relative orientations for in-plane and out-of-plane measurements. Diffraction angles are exaggerated for demonstration.

locations, middle (M), cathode (C) and anode (A), as shown in Fig. 1a.

In-plane and out-of-plane measurements

For *in-plane* measurements, the incident and diffracted beams were in the same plane as the battery electrodes. When the diffraction vector is perpendicular to the sheets of the battery electrodes, they are referred to as *out-of-plane* measurements (Fig. 1c). These two orthogonal directions of strain measurements within the battery were designed to examine the effect of texture and electrode sheet orientation.

Results

The goal of these experiments is to measure the strain in different regions of the battery to identify sections of the battery that were underperforming or failing. In Fig. 3, the change in interplanar spacing is shown for the graphite anode corresponding to the stage of

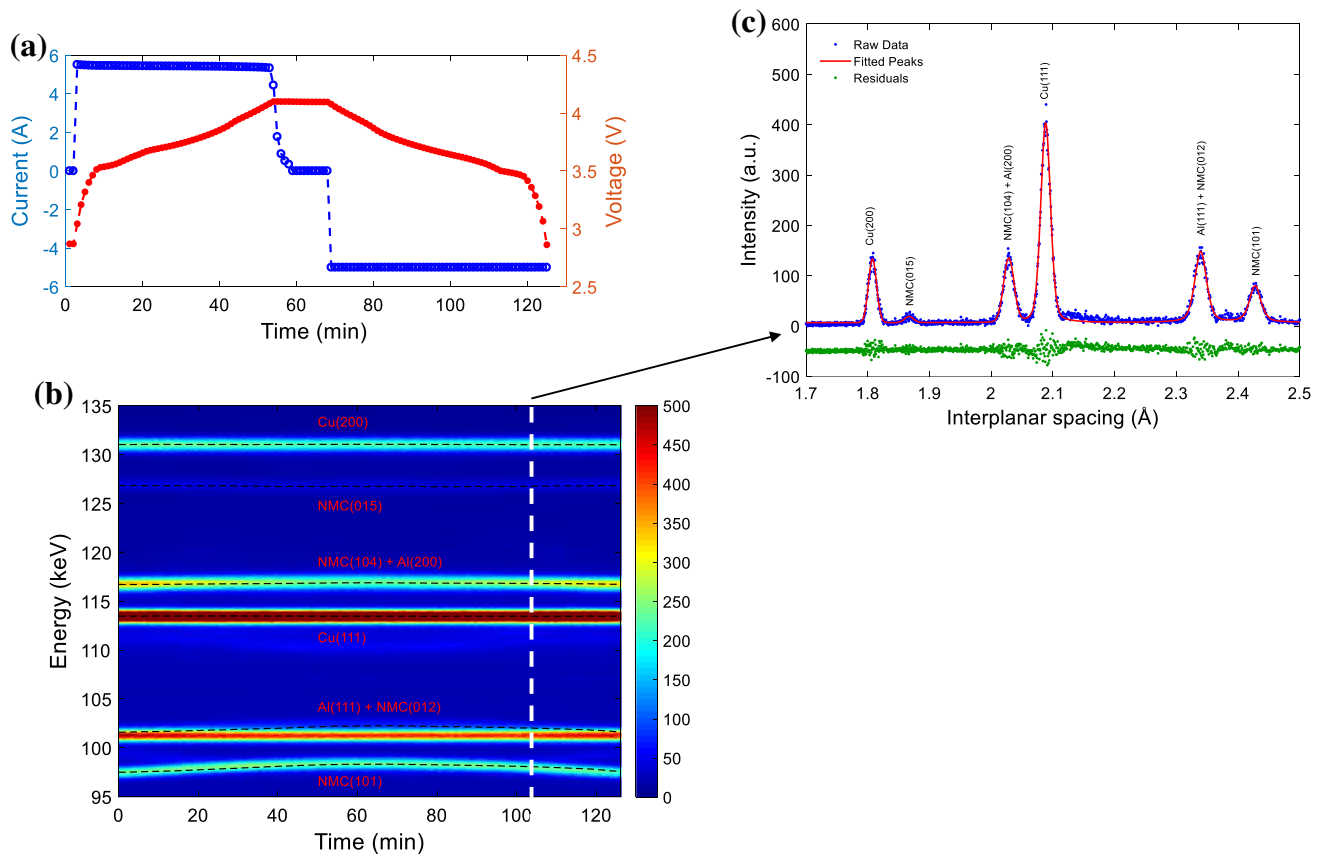


Figure 2 **a** Typical full charge–discharge cycle for 5 Ah battery at 1 C. **b** Contour plot of a select region in reciprocal space during charge–discharge cycle. **c** Selected spectrum at a discharged stage, with fitting and remaining residuals.

Table 1 Miller indices with corresponding d -spacing for anode, cathode and current collectors in the energy range under current study

Material	Interplanar spacing (Å)	($h k l$)
NMC	2.438	1 0 1
NMC	2.337	0 1 2
NMC	2.031	1 0 4
NMC	1.867	0 1 5
C	3.355	0 0 2
LiC ₁₂	3.518	0 0 2
Cu	2.080	1 1 1
Cu	1.802	2 0 0
Cu	1.274	2 2 0
Al	2.339	1 1 1
Al	2.025	2 0 0

charge. Notably, a much stronger intensity of graphite is observed for *out-of-plane* measurements compared to *in-plane* measurements (Fig. 4). For the *out-of-plane* measurements, the peaks corresponding

to LiC₁₂, LiC₂₄ and graphite appear as step functions in the graph, whereas for *in-plane* measurements, there is a relatively continuous transition from one phase to another.

The literature [2, 17, 25, 27–31] suggests that graphite layers are highly orientated with the ‘ c ’ axis perpendicular to the plane of the current collector such that lithium atoms intercalate between the carbon layers that are oriented along the c -axis. The orientation becomes more pronounced when the sheets are pressed during the compaction of battery electrode layers which is the reason for the low intensity of $\langle 0 0 n \rangle$ planes of graphite during *in-plane* measurements.

For the case of the Li-NMC cathode, the lattice parameter ‘ c ’ expands, while ‘ a ’ shrinks during the charge, and this trend reverses during discharge, shown in Fig. 5. This observation agrees with previous reports [32–34], where the lattice expansion in ‘ c ’ follows linearly with the intercalation of lithium up to 90% of charge before leveling off. It has been

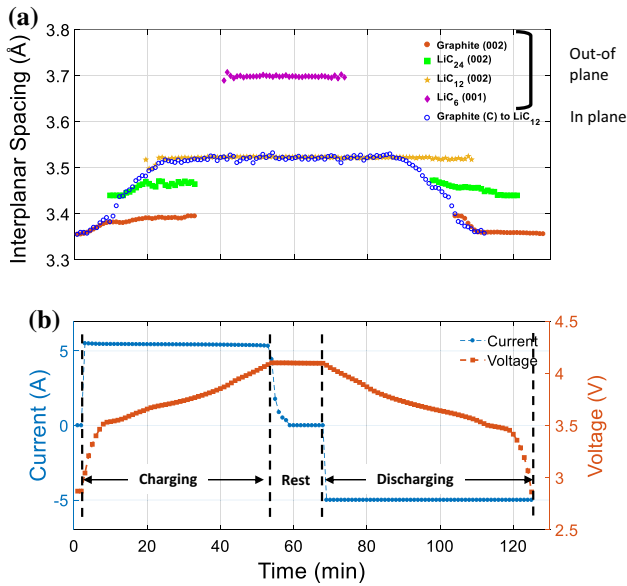


Figure 3 **a** Measured lattice parameters for the anode (graphite and Li-graphite) peaks with charge-discharge rate of 1 C for the central section of the battery, position M2 (see Fig. 1). **b** A typical battery *I*-*V* characteristic plot.

suggested by Dolotko et al. [32] that initial lithium diffusion is accommodated by a change in the oxidation state of Ni⁴⁺ to Ni²⁺, but as the *c/a* ratio deviates from linearity (Fig. 5c), a phase transformation occurs which changes the bonding environment and oxidation state of Co [8]. Mn is believed to be electronically inactive and a stabilizer of the crystal structure, which is a crucial factor for a safe battery. Since the battery was in use before the current set of experiments, no irrecoverable loss was observed during the cycle, as is seen in the first discharge of a new battery [8]. During discharge, Li moves from anode to cathode which changes the stoichiometry of the Li-NMC cathode. Based on the calculated lattice parameters, the cathode stoichiometry is found to change from Li_{0.85}Ni_{1/3}Mn_{1/3}Co_{1/3}O₂ and Li_{0.35}Ni_{1/3}Mn_{1/3}Co_{1/3}O₂ for fully discharged and charged states, respectively [12, 36, 37]. Unlike the anode, the cathode (Li-NMC) does not show any preferred orientation for *in-plane* and *out-of-plane* as supported by the literature [18] since grains of Li-NMC were found

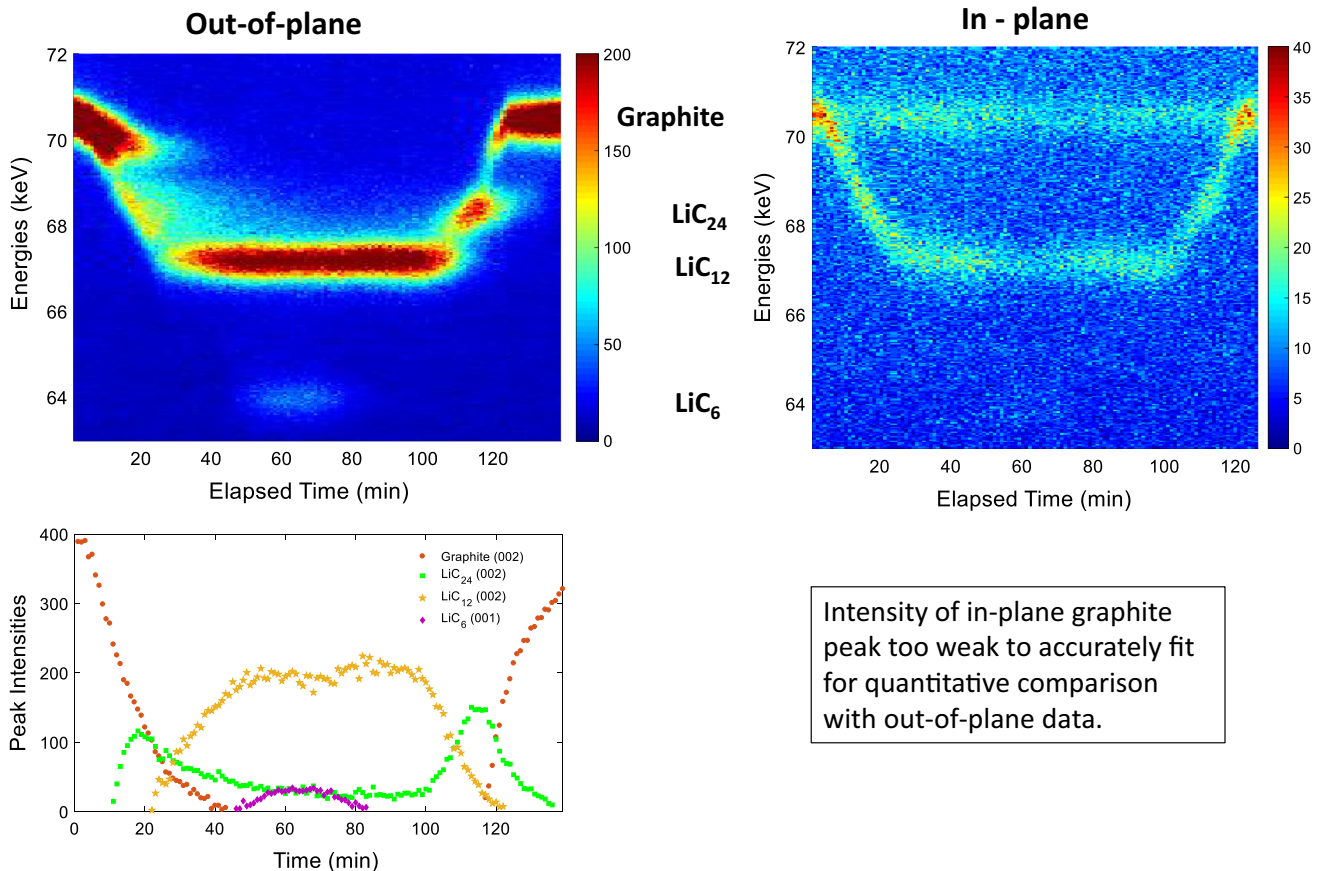


Figure 4 Comparison of graphite and Li-C phases, out-of-plane and in-plane peak intensities indicates orientation of the graphite (002) planes.

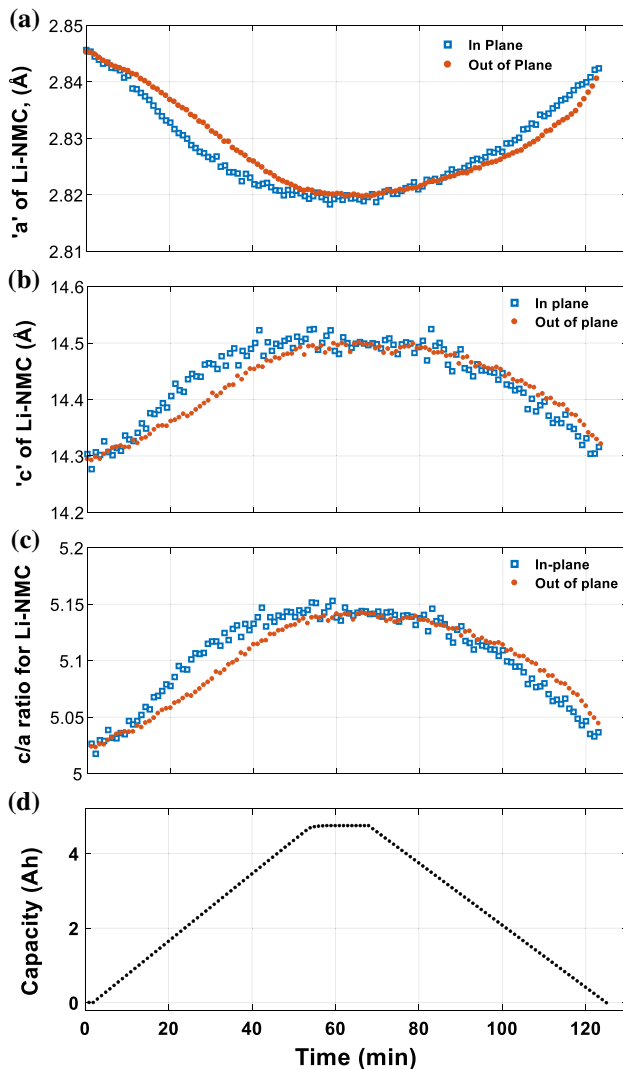


Figure 5 Change of lattice parameters **a** 'a', **b** 'c' and **c** ratio of *c/a* taken at M2 of the battery, using peaks (101) and (015) during a 1 C charge–discharge cycle. Subplot **d** gives the capacity of the battery as it is charged and discharged with time. The battery has already lost its full capacity since it switches from discharging at 5 A to rest in less than an hour of continuous use.

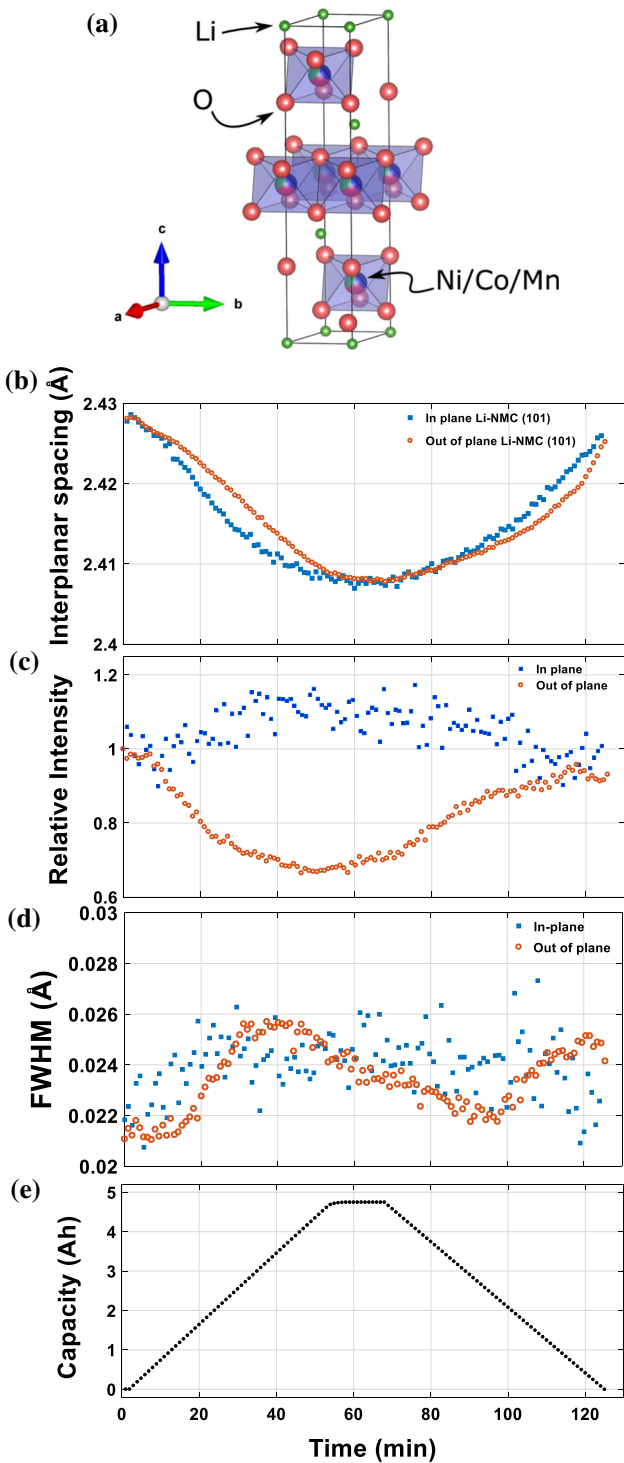
to be equiaxed. This indicates isotropic macroscopic expansion and contraction during battery cycling.

Figure 6 shows a detailed study of full width at half maximum (FWHM) and normalized relative intensity for the cathode (101) for *in-plane* and *out-of-plane* configurations. There is a slight difference in the *d*-spacing for the two cycles, which may have been the result of the battery being stored idle for 4 months between two runs at the synchrotron. While the intensity of the (101) peak for *in-plane* measurements stays relatively constant, the out-of-plane normalized intensity drops to 0.65 of its initial

intensity. Similar patterns were noticed by Paxton et al. [24] which were related to the physical movement of layers due to mechanical stress. As the layers of the cathode moved out of the gauge volume, the intensity of the peaks decreased. No discernable trend was seen in elastic strain as estimated from the full width at half maximum (FWHM) of the peak.

Referring to Fig. 1a, the cathode (positive), anode (negative) and middle sections of the battery were investigated to compare the relative responses during charging and discharging. It was found that while the majority of the battery functioned as expected the negative end of the battery had a non-uniform response, as indicated in Fig. 7. Utilizing strain in the lattice related to the state of charge, a lag during charging is observed. This section of the battery did not undergo complete discharge as a good contact between anode and cathode is constrained by the dog-bone structure of the wrapped cell stack. This contact problem gets worse over the lifetime of the battery, which has been indicated by the presence of an inactive cathode (Li-NMC) in Figs. 7 and 8.

Profile measurements were taken by scanning across the thickness of the battery to compare the response of the middle region of the battery with the region near the negative terminal, the anode side of the battery. Results from Fig. 9 confirm the earlier finding that while all of the layers of the middle section (M) of the battery were lithiating and delithiating to the same extent, the negative end, A, shows variability across the layers, from A1 to A6, while the outermost layer (A1) neither lithiates nor delithiates completely and layers at A2, A5 and A6 do not return to their initial state at the end of the cycle. The middle layers, A3 and A4, behaved as expected. Another interesting observation is that although A1 is symmetrical to A6, the strain in the two sections are different. This may be the result of the assembly design. The prismatic battery assembly involves jelly rolling the layers into a spiral with two bends (a link showing the design is embedded in ref [38]). The strain at one face of the battery will differ from the other end because the boundary condition changes from near no strain under loop stress to no stress at the free end. The analytical and numerical stress analysis is part of a future work. Interestingly, these lattice strains recovered quickly after the battery was put in its rest state. This suggests that the outermost battery layers have poor point of contact to sustain the steady exchange of lithium ion at the interface



◀ **Figure 6** a Unit cell of Li-NMC generated by VESTATM [35] and the CIF number 4002443 with space group R-3 m [16]. Interplanar spacing (b), peak intensity (c) and full width at half maxima (d) of cathode peak (101). A corresponding state of charge for battery during the charge and discharge cycle is shown in e. No significant elastic deformation is observed from FWHM analysis suggesting the cathode remains relatively stable during the cycling. The drop in intensity for out-of-plane measurements comes from the physical movement of the battery layers during the charge–discharge cycle since the electrode sheets are perpendicular to the plane of the X-ray direction and diffracted beam [24].

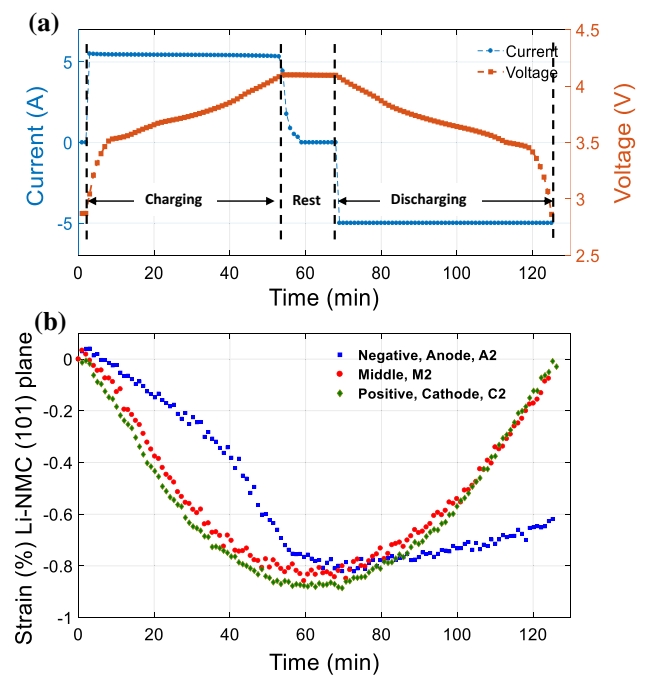


Figure 7 a Voltage–current characteristic plot of battery during the cycling. b Comparison of strain in NMC (1 0 1) plane near negative, middle and positive electrodes of the battery. The negative end does not charge or discharge to its full extent resulting in loss of capacity over time. Similar observations were made for the negative terminal (see Fig. 8).

during operation. However, once the battery goes to ‘rest’ state, lithium ions move along the sheets to maintain equipotential in the cathode and anode. This local ‘delamination’ does not cause permanent loss in battery capacity, but could be one of the primary factors of battery degradation over long run. This quick recovery highlights the importance of in situ diffraction techniques to study the strain measurements directly and nondestructively during operation.

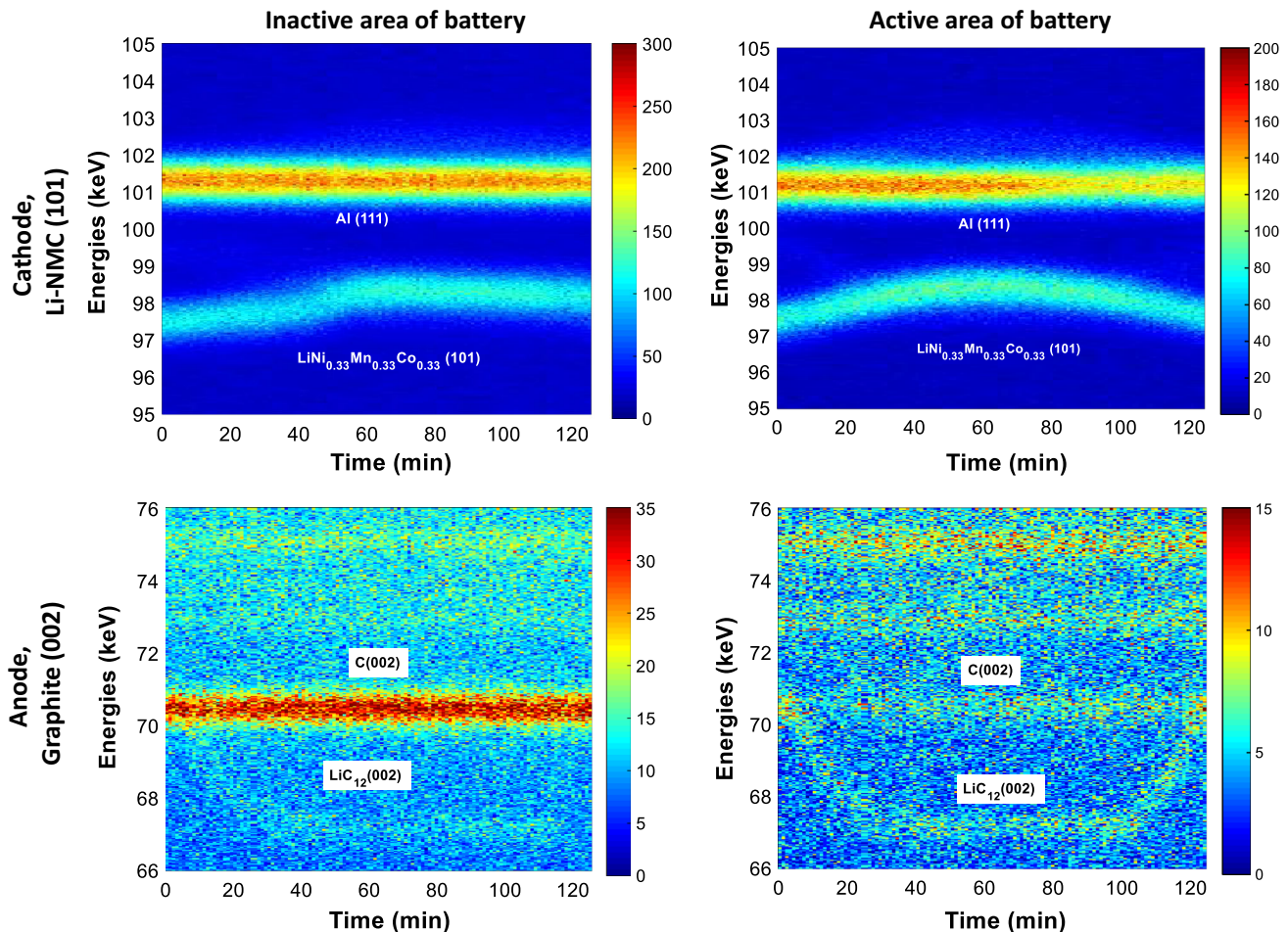


Figure 8 Comparison of cathode and anode at the negative end (inactive area) and middle section (active area) of the battery. The inactive area of the battery shows no intercalation of Li in graphite as well as delayed shift of the Li-NMC [1 0 1] peak.

Batteries are customarily tested in continuous charge and discharge at a slower rate such as 1 C to measure their performance at equilibrium. Pulse (or burst) discharge is normally discouraged as it exceeds the sustainable rate of discharge and adversely affects the battery's longevity. Depending on the level and duration of the stress during high current discharge, the battery's capacity has been reported [39] to drop to 2% compared to constant current discharge. The battery was tested at 4 C (20 A current), and the analysis followed the change in the (101) interplanar spacing of the Li-NMC cathode. During high current rate experiments, the interplanar spacing and hence the strain change four times faster for a 4 C discharge rate compared to 1 C. This will cause peak broadening for the same acquisition time of X-ray diffraction. Hence, the accuracy in measurement is lowered for faster processes. After removing the load, the battery electrical potential

gradually recovered as can be seen in Fig. 10. When the strain resulting from the pulse discharge in the battery is analyzed, it is observed that even though the battery is in its rest state, the Li-NMC cathode continues to take in lithium at a higher rate compared to the discharge rate of 1 C. In other words, the recovery rate of strain for pulse discharge is higher than the normal discharge rate, which is expected as the battery was forced to operate at high power in pulse mode, beyond its equilibrium condition.

Heat generation during continuous use of the battery has been suggested to negatively affect the battery life [40]. To understand this effect, the lattice parameters of the cathode were compared before and after a continuous use of the battery for 24 h at a rate of 1 C for the same state of discharge of the battery (at complete discharge state). The values were found to be comparable, suggesting that the thermal contribution for continuous use of the battery at 1 C is not a

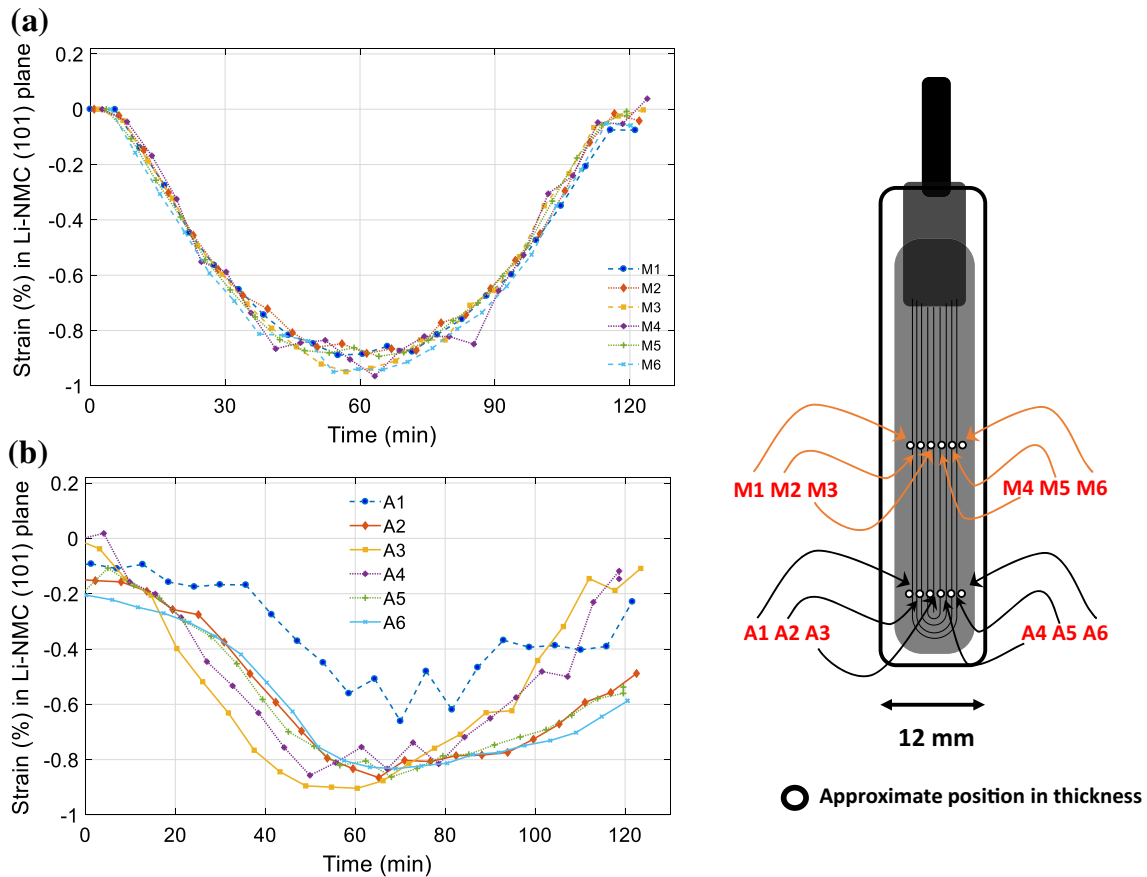


Figure 9 Comparison of the strain profile at the **a** middle and **b** negative (anode) ends of the battery. While the center of the battery has no deterioration, the outer sheets of the negative end are already losing capacity, with varying state of charge across the thickness.

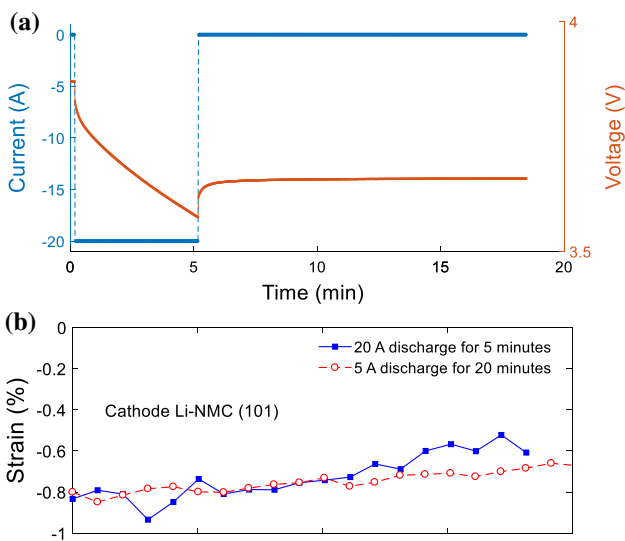


Figure 10 **a** Pulse discharge of the battery at 20 A for 5 min and its effect on the battery continued to be seen in terms of **b** strain recovery in the cathode for more than 15 min after the battery was brought to rest. For comparison another discharge cycle at 5 A is shown.

significant degradation mechanism that can be measured by residual stress for the battery.

Discussion

Scaling up the capacity of Li-ion rechargeable batteries from low-power consumer devices to high-power devices such as automobiles comes with many engineering challenges. To build a higher capacity battery, larger and greater numbers of layers in the battery stacks are needed. Layers in prismatic batteries are tightly compressed to maintain stack pressure so that the battery layers stay in contact during cycling. Cycling induces mechanical stresses in the battery layers and may damage the electrodes and alter the structure of the battery components during each cycle. The relative expansion of the layers of different battery components introduces stresses at the interfaces whose effects can build up over time and lead to increasing damage to the battery layer

structures. The jelly roll structure used in this battery cell design appears to create regions of poor cyclability in the regions of high curvature. This situation may be worsened as more battery layers are added, limiting the possibility of scaling. To understand this problem better, an analytical stress analysis and node base simulation is needed, which is beyond the scope of this work.

Conclusion

The structural changes in the cathode and anode of the 5 Ah Li-NMC battery were investigated using in situ energy-dispersive X-ray diffraction to track the movement of lithium between the anode and cathode during the charge–discharge cycle, using *in-plane* and *out-of-plane* measurements. We observe that the graphite is highly oriented with the ‘*c*’ axis perpendicular to the plane of the electrode sheet, which expands to accommodate the lithium. The $\text{Li}_x\text{Ni}_{0.33}\text{Mn}_{0.33}\text{Co}_{0.33}\text{O}_2$ cathode expands along its ‘*c*’ axis and contracts in its ‘*a*’ axis during the charging cycle. However, random orientation of the grains of Li-NMC makes this expansion isotropic on the macroscopic level [18]. While most measured regions of the battery had completely reversible cycles, we observed irregular cycling behavior at the bottom of the negative terminal, believed to be caused by poor local contact of the battery layers. The profile scan across the thickness of the battery confirms that the outermost layers at the negative end of the battery cycle non-uniformly. Pulse discharge of the battery at the rate of 4 C (20 A) shows a non-equilibrium strain in the cathode, which continues to recover for a considerably long time after the current stops flowing, demonstrating the detrimental nature of burst-mode discharge and, therefore, is strongly discouraged. This work also highlights the versatility of EDXRD measurements in strain analysis as well as for identification of phase changes of individual materials in multicomponent systems for different charge rates.

Acknowledgements

The authors wish to express their gratitude for the financial support provided by the Office of Naval Research (ONR) and Dr. Antti Makineen under

Contract No. N00014-15-1-2492. This research used resources of the Advanced Photon Source, a U.S. Department of Energy (DOE) Office of Science User Facility operated for the DOE Office of Science by Argonne National Laboratory under Contract No. DE-AC02-06CH11357.

Compliance with ethical standards

Conflict of interest All authors declare that they have no conflict of interest.

References

- [1] Kempener R, Borden E (2015) Battery storage for renewables: market status and technology outlook. IRENA International Energy Storage Policy and Regulation, Abu Dhabi
- [2] Sakti A, Michalek JJ, Fuchs ER, Whitacre JF (2015) A techno-economic analysis and optimization of Li-ion batteries for light-duty passenger vehicle electrification. *J Power Sources* 273:966–980
- [3] Chiang Y-M (2010) Building a better battery. *Science* 330:1485–1486
- [4] Doeff MM, Brodd RJ (2013) Battery cathode, in batteries for sustainability: selected entries from the encyclopedia. R.A. Meyers, New York
- [5] Fu K, Gong Y, Liu B et al (2017) Toward garnet electrolyte-based Li metal batteries: an ultrathin, highly effective, artificial solid-state electrolyte/metallic Li interface. *Sci Adv* 3(4):e1601659
- [6] Han X, Gong Y, Fu K et al (2017) Negating interfacial impedance in garnet-based solid-state Li metal batteries. *Nat Mater* 16(5):572–579
- [7] Tarascon JM, Armand M (2010) Issues and challenges facing rechargeable lithium batteries. In: Dusastre V (ed) *Materials for sustainable energy*. Co-Published with Macmillan Publishers Ltd, London, pp 171–179
- [8] Buchberger I, Seidlmayer S, Pokharel A, Piana M, Hattendorf J, Kudejova P, Gilles R, Gasteiger HA (2015) Aging analysis of graphite/LiNi_{1/3}Mn_{1/3}Co_{1/3}O₂ cells using XRD, PGAA, and AC impedance. *J Electrochem Soc* 162(14):A2737–A2746
- [9] Vetter J (2005) Ageing mechanisms in lithium-ion batteries. *J Power Sources* 147(1):269–281
- [10] Newman J (1995) Optimization of porosity and thickness of a battery electrode by means of a reaction-zone model. *J Electrochem Soc* 142(1):97–101
- [11] Padhi AK, Nanjundaswamy KS, Goodenough JB (1997) Phospho-olivines as positive-electrode materials for

- rechargeable lithium batteries. *J Electrochem Soc* 144(4):1188–1194
- [12] Albertini VR, Perfetti P, Ronci F, Reale P, Scrosati B (2001) In situ studies of electrodic materials in Li-ion cells upon cycling performed by very-high-energy X-ray diffraction. *Appl Phys Lett* 79(1):27–29
- [13] Glazer MPB, Okasinski JS, Almer JD, Ren Y (2016) High-energy X-ray scattering studies of battery materials. *MRS Bull* 41(06):460–465
- [14] Iizumi M (1986) Real-time neutron diffraction studies of phase transition kinetics. *Physica B + C* 136(1):36–41
- [15] Lin F, Liu Y, Yu X et al (2017) Synchrotron X-ray analytical techniques for studying materials electrochemistry in rechargeable batteries. *Chem Rev* 117(21):13123–13186
- [16] Taminato S, Yonemura M, Shiotani S et al (2016) Real-time observations of lithium battery reactions-operando neutron diffraction analysis during practical operation. *Sci Rep* 6:28843
- [17] Trucano PC, Chen R (1975) Structure of graphite by neutron diffraction. *Nature* 258:136–137
- [18] Yin SC, Rho YH, Swanson I, Nazar LF (2006) X-ray/neutron diffraction and electrochemical studies of lithium De/Re-Intercalation in $\text{Li}_{1-x}\text{Co}_{1/3}\text{Ni}_{1/3}\text{Mn}_{1/3}\text{O}_2$ ($x = 0 \rightarrow 1$). *Chem Mater* 18(7):1901–1910
- [19] Allen MG, Mehregany M, Howe RT, Senturi SD (1987) Microfabricated structures for the in situ measurement of residual stress, Young's modulus, and ultimate strain of thin films. *Appl Phys Lett* 51(4):241–243
- [20] Covey-Crump SJ, Schofield PF, Stretton IC, Daymond MR, Kight KS, Tant J (2013) Monitoring in situ stress/strain behaviour during plastic yielding in polymineralic rocks using neutron diffraction. *J Struct Geol* 47:36–51
- [21] Croft M, Zhong Z, Jiswawi N, Zakharchenko I, Holtz RL, Skaritka J, Fast T, Sadananda K, Lakshminpathy M, Tsakalakos T (2005) Strain profiling of fatigue crack overload effects using energy dispersive X-ray diffraction. *Int J Fatigue* 27(10):1408–1419
- [22] Daymond MR, Bourke MAM, Von Dreele RB, Clausen B, Lorentzen T (1997) Use of Rietveld refinement for elastic macrostrain determination and for evaluation of plastic strain history from diffraction spectra. *J Appl Phys* 82(4):1554–1562
- [23] Paxton WA, Akdoğan EK, Şavkliyildiz I, Chokshi AU, Silver SX, Tsakalakos T, Zhong Z (2014) Asynchronous stoichiometric response in lithium iron phosphate batteries. *J Mater Res* 30(3):417–423
- [24] Paxton WA, Zhong Z, Tsakalakos T (2015) Tracking inhomogeneity in high-capacity lithium iron phosphate batteries. *J Power Sources* 275:429–434
- [25] Billaud D, Henry FX, Lelaurian M, Wilmann P (1996) Revisited structures of dense and dilute stage II lithium-graphite intercalation compounds. *J Phys Chem Solids* 57(6):775–781
- [26] Park JS, Okasinski J, Chatterjee K, Chen Y, Almer J (2017) Non-destructive characterization of engineering materials using high-energy X-rays at the advanced photon source. *Synchrotron Radiat News* 30(3):9–16
- [27] Wang XL, An K, Cai L et al (2012) Visualizing the chemistry and structure dynamics in lithium-ion batteries by in situ neutron diffraction. *Sci Rep* 2:747
- [28] Dahn JR, Fong R, Spoon MJ (1990) Suppression of staging in lithium-intercalated carbon by disorder in the host. *Phys Rev B* 42(10):6424–6432
- [29] Majid N, Hafiz S, Arianto S et al (2016) Analysis of effective pulse current charging method for lithium ion battery. *J Phys Conf Ser* 817:012008
- [30] Guerard D, Herold A (1975) Intercalation of lithium into graphite and other carbons. *Carbon* 13(4):337–345
- [31] Ogumi Z, Inaba M (1998) electrochemical lithium intercalation within carbonaceous materials: intercalation process, surface film formation, and lithium diffusion. *Bull Chem Soc Jpn* 71(14):521–534
- [32] Dolotko O, Senyshyn A, Muhlbauer MJ, Nikolowski K, Ehrenberg H (2014) Understanding structural changes in NMC Li-ion cells by in situ neutron diffraction. *J Power Sources* 255:197–203
- [33] Gu YJ, Chen YB, Liu HQ, Wang YM, Wang CL, Wu HK (2011) Structural characterization of layered $\text{LiNi}_{0.85-x}\text{Mn}_x\text{Co}_{0.15}\text{O}_2$ with $x = 0, 0.1, 0.2$ and 0.4 oxide electrodes for Li batteries. *J Alloys Compd* 509(30):7915–7921
- [34] Kim JM, Chung HT (2004) The first cycle characteristics of $\text{Li}[\text{Ni}_{1/3}\text{Co}_{1/3}\text{Mn}_{1/3}]\text{O}_2$ charged up to 4.7 V. *Electrochim Acta* 49(6):937–944
- [35] Momma K, Izumi F (2011) VESTA 3 for three-dimensional visualization of crystal, volumetric and morphology data. *J Appl Crystallogr* 44(6):1272–1276
- [36] Liao PY, Duh JG, Lee JF, Sheu HS (2007) Structural investigation of $\text{Li}_{1-x}\text{Ni}_{0.5}\text{Co}_{0.25}\text{Mn}_{0.25}\text{O}_2$ by in situ XAS and XRD measurements. *Electrochim Acta* 53(4):1850–1857
- [37] Mohanty D, Sefat AS, Kalnaus S, Li J, Meisner RA, Payzant EA, Abraham DP, Wood DL, Daniel C (2013) Investigating phase transformation in the $\text{Li}_{1.2}\text{Co}_{0.1}\text{Mn}_{0.55}\text{Ni}_{0.15}\text{O}_2$ lithium-ion battery cathode during high-voltage hold (4.5 V) via magnetic, X-ray diffraction and electron microscopy studies. *J Mater Chem A* 1(20):6249–6261
- [38] Christopher Arcus, Lithium Batteries—Clues To The Mystery. <https://cleantechnica.com/files/2018/02/battery-cell-shapes.jpg>. Accessed 6 Sept 2018

- [39] Hooper A, Powell RJ, Marshall TJ, Neat RJ (1989) Pulse discharge characteristics of solid-state lithium batteries. *J Power Sources* 27(1):3–13
- [40] Leng F, Tan CM, Pecht M (2015) Effect of temperature on the aging rate of Li ion battery operating above room temperature. *Sci Rep* 5:12967